A Comparison study of Drag correlations for a Dispersed Multiphase flow in a Fluidized bed

M Siva Karthikeya

Department of Aerospace Engineering

SASTRA Deemed University, Thanjavur, Tamilnadu, India

Abstract

The present study employs the open-source CFD toolbox, OpenFOAM, to investigate the effect of various drag correlations in the literature on the Mean Eulerian particle velocity distribution of the gas-solid fluidized bed. Superficial gas velocities of 2.19 m/s and 3.28 m/s are considered at the inlet for the transient multiphase simulation. The time-averaged particle velocity is estimated at five lateral locations of the fluidized bed for validation against the experimental data of the National Energy Technology Laboratory (NETL). Finally, the particle velocity distribution is compared between a drag correlation given by Syamlal O'Brien and two combined drag correlations of Gidaspow.

Keywords: OpenFOAM, CFD, Fluidized bed, Multiphase

1. Introduction

Research on sustainable technologies has burgeoned in the 21st century to tackle environmental degradation occurring at every stage of any industrial process. Fluidized bed technology is one such potential deployment into the category of sustainable technologies, widely used in the petroleum, pharmaceutical, chemical, and many other industries and has been at a focal point of research. With the primary function of making a solid-fluid mixture behave as a fluid, this technology has the potential to reduce the harmful gas emissions from industries without compromising on the efficiency of results like combustion, catalytic cracking, and other chemical processes. Therefore, it is important to develop computational models to predict the flow characteristics inside the fluidized bed for further development.

2. Problem Statement

The key objective of the present study is to identify the most reliable drag correlation for computational modelling of Multiphase flows, particularly dispersed flows. To implement various drag correlations and analyse the results, a 2D Fluidized bed was considered the most suitable case for three important reasons.

1. Standard case of a dispersed flow
2. Availability of reliable experimental data to validate
3. Computationally less expensive for a Multiphase simulation
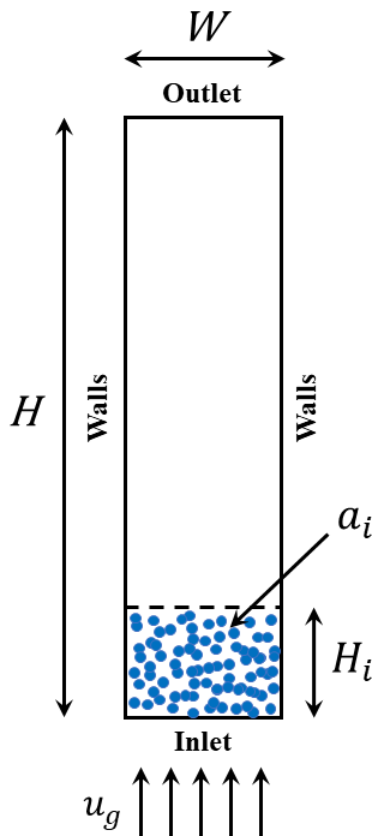
Parameters	Value
Column height (H)	1.22 m
Column width (W)	0.23 m
Static bed height (H_i)	0.173 m
Initial packing fraction (a_i)	0.58
Superficial gas velocity (u_g)	2.19 m/s & 3.28 m/s
Gas density (ρ_g)	1.204 kg/m^3
Particle diameter (d_p)	3256 μm
Particle density (ρ_p)	1131 kg/m^3
Gravitational acceleration (g)	9.81 m/s

Table 1: Dimensions and parameters used in this study

Figure 1: Fluidized bed model

The geometry and boundaries of the 2D fluidized bed used for this study are shown in Figure 1. The corresponding dimensions and few parameters like the superficial gas velocity at the inlet, the initial packing fraction of the dispersed phase (particles) are mentioned in Table 1. An initial packing fraction of 0.58 means that 58% of the static bed is occupied with the dispersed phase (particles) and the remaining 42% with the continuous phase (liquid). In this study of the two-phase flow inside the fluidized bed for various drag correlations, the *twoPhaseEulerFoam* solver is used.

3. Governing Equations

Multiphase flows are numerically modelled using different approaches such as:

1. Direct Numerical Simulation (DNS)
2. Eulerian – Langrangian approach
3. Eulerian – Eulerian approach

Eulerian – Eulerian approach is further classified based on the phase morphology into separated and dispersed systems [1]. The fluidized bed being a dispersed system, multi-fluid modelling is used where both phases are treated as interacting and interpenetrating continua, therefore, share the same basic continuity and momentum equations for each phase individually as shown in Eqs. (1), (2), and (4). For the solid phase, the Kinetic Theory of Granular Flow (KTGF) [2] was adopted for closure which considers the conservation of Solid Fluctuation Energy. KTFG approach is an extension to the classical kinetic theory of gases to dense particulate flows, where the fluctuation energy is described with the help of granular temperature (θ).

Three important assumptions made in this study for simplification are:

1. Both solid and liquid phases are isothermal.
2. There is no interphase mass transfer between both phases.
3. Solid particles are of pure spherical configuration with a mean diameter and density.

- Conservation of Mass (k = f for fluid phase, k = s for solid phase)

$$\frac{\partial}{\partial t}(\alpha_k \rho_k) + \frac{\partial}{\partial x}(\alpha_k \rho_k \boldsymbol{u}_k) = 0 \tag{1}$$

- Conservation of Momentum (fluid phase)

$$\frac{\partial}{\partial t}(\alpha_f \rho_f \boldsymbol{u}_f) + \nabla \cdot (\alpha_f \rho_f \boldsymbol{u}_f \boldsymbol{u}_f) = \alpha_f \nabla \cdot \bar{\boldsymbol{\tau}}_f + \alpha_f \rho_f \boldsymbol{g} - \alpha_f \nabla p - \boldsymbol{F}_{df} - \boldsymbol{F}_{vm} - \boldsymbol{F}_{lf} \tag{2}$$

$\boldsymbol{F}_{df}, \boldsymbol{F}_{vm}, \boldsymbol{F}_{lf}$ is the drag force, virtual mass force, and lift force respectively in both equations (2) and (4). Since drag force contributes predominantly to the momentum exchange between the fluid and solid phases, it is given more importance in this study.

The stress tensor of the liquid phase from Eq. (2) is expanded in Eq. (3)

$$\bar{\boldsymbol{\tau}}_f = \mu_f \left[\nabla \boldsymbol{u}_f + (\nabla \boldsymbol{u}_f)^T \right] - \frac{2}{3} \mu_f (\nabla \cdot \boldsymbol{u}_f) \bar{\boldsymbol{I}} \tag{3}$$

where μ_f is the combined turbulent and laminar viscosity for the fluid phase. Further, $k-\varepsilon$ turbulence model is used in the study for the fluid phase.

- Conservation of Momentum (solid phase)

$$\frac{\partial}{\partial t}(\alpha_s \rho_s \boldsymbol{u}_s) + \nabla \cdot (\alpha_s \rho_s \boldsymbol{u}_s \boldsymbol{u}_s) = -\alpha_s \nabla p - \nabla p_s + \nabla \cdot \bar{\boldsymbol{\tau}}_s + \alpha_s \rho_s \mathbf{g} + \boldsymbol{F}_{df} + F_{vm} + F_{lf} \tag{4}$$

The solid phase stress tensor is expressed in terms of bulk solid viscosity ξ_s, and shear solid viscosity μ_s in Eq. (5)

$$\bar{\boldsymbol{\tau}}_s = \mu_s \left\{ [\nabla \boldsymbol{u}_s + (\nabla \boldsymbol{u}_s)^T] - \frac{2}{3}(\nabla \cdot \boldsymbol{u}_s) \bar{\boldsymbol{I}} \right\} + \xi_s \nabla \cdot \boldsymbol{u}_s \bar{\boldsymbol{I}} \tag{5}$$

- Conservation of Solid Fluctuation Energy

$$\frac{3}{2} \left[\frac{\partial}{\partial t}(\alpha_s \rho_s \theta) + \nabla \cdot (\alpha_s \rho_s \theta) \boldsymbol{u}_s \right] = \left(-\nabla p_s \bar{\boldsymbol{I}} + \bar{\boldsymbol{\tau}}_s \right) : \nabla \boldsymbol{u}_s + \nabla \cdot (k_s \nabla \theta) - \gamma_s - 3\beta\theta + D_{l_s} \tag{6}$$

Granular temperature is used to measure the energy of fluctuating velocity of particles. In our case, the *equilibrium* condition is set to *off* in turbulent properties of particles, enabling the solver to solve algebraic equations of granular temperature.

3.1 Drag correlations

Numerous drag correlations are available in the literature [1] that can model the mechanism of interphase momentum transfer majorly caused due to drag force between the phases. A thorough literature study was performed to identify such drag correlations that could model the flow for all packing fraction regimes, individually or as a combination of two. It is important for a drag correlation to accurately predict the flow at all packing fraction regimes because, the probability of a cell in a domain, especially at the interface, to overshoot the maximum packing fraction of the domain can never be neglected and must be taken into account. Also, the correlations adopted must be applicable for a multi-particle system to consider the effect of other particle's presence. Upon considering such crucial factors, three drag correlations were chosen to model the two-phase flow inside a fluidized bed.

a) Gidaspow-Ergun-Wen-Yu:

This is a combination of the Ergun drag correlation applicable for dense systems and the Wen Yu correlation that can model a dilute flow where viscous forces are dominant, accurately.

This correlation uses the Ergun equation, Eq. (7), for $\alpha_p \geq 0.2$ and the Wen–Yu equation, Eq. (8) for $\alpha_p \leq 0.2$, where K is defined as the drag function for each correlation. Drag force in the Ergun correlation is calculated based on pressure drop per unit length, Eq. (9), unlike the Wen Yu correlation that considers the drag coefficient on a single particle, Eq. (10).

$$K = 150 \frac{\mu_g}{d_p} \frac{\alpha_p^2}{(1-\alpha_p)^2} + 1.75 \frac{\rho_g U_r}{d_p} \frac{\alpha_p^2}{(1-\alpha_p)^2} \tag{7}$$

$$K = \frac{3}{4d_p} C_{Ds} \alpha_p (1-\alpha_p) \rho_g U_r (1-\alpha_p)^{-2.65} \tag{8}$$

$$\frac{\Delta p}{L} = 150 \frac{\mu_g U_r}{d_p g} \frac{\alpha_p^2}{(1-\alpha_p)^3} + 1.75 \frac{\rho_g U_r^2}{d_p g} \frac{\alpha_p}{(1-\alpha_p)^3} \tag{9}$$

$$C_{Ds} = \begin{cases} \frac{24}{\text{Re}}(1 + 0.15\text{Re}^{0.687}), & \text{Re} \leq 1000 \\ 0.44, & \text{Re} > 1000 \end{cases} \tag{10}$$

b) Gidaspow-Schiller-Naumann:

This drag correlation is capable of calculating the drag in a multi-particle system, unlike the Schiller-Naumann correlation which is restricted to a single particle system only. The drag function for this correlation is defined in Eq. (11). Schiller-Naumann drag coefficient, Eq. (10), is used by replacing the Re with $(1 - \alpha_p)$Re, as shown in Eq. (12) below.

$$K = \frac{3}{4d_p} C_{Ds}\alpha_p(1 - \alpha_p)\rho_l U_r(1 - \alpha_p)^{-2.65} \tag{11}$$

$$C_{Ds} = \begin{cases} \dfrac{24}{(1 - \alpha_p)\text{Re}}\left(1 + 0.15\left((1 - \alpha_p)\text{Re}\right)^{0.687}\right), \text{Re} \leq 1000 \\ 0.44, \hspace{4.5cm} \text{Re} > 1000 \end{cases} \tag{12}$$

c) Syamlal O'Brien

This drag correlation is based on the primary assumption that the Archimedes number remains the same for terminal settling velocity for both single and multi-particle systems. It uses the expression, Eq. (13), to relate the settling velocity and the void fraction, where Re_s is the Reynolds number for a single particle and V_r, the ratio of terminal settling velocity in a multi-particle system to that of a single particle system.

$$\frac{V_r - A}{B - V_r} = 0.06\text{Re}_s \tag{13}$$

$$V_r = 0.5\left(A - 0.06\text{Re} + \sqrt{(0.06\text{Re})^2 + 0.12\text{Re}\,(2B - A) + A^2}\right) \tag{14}$$

$$A = (1 - \alpha_p)^{4.14} \tag{15}$$

$$B = \begin{cases} C_1(1 - \alpha_p)^{1.28}, \alpha_p \geq 0.15 \\ (1 - \alpha_p)^{C_2}, \alpha_p < 0.15 \end{cases} \tag{16}$$

Eq. (14), (15), and (16) are obtained by solving Eq. (13) after replacing Re_s with Re/V_r. Drag coefficient proposed by Dallavalle, Eq. (17), is used here to obtain the final drag function in Eq. (18), where $\mathbf{U}_r$ is the relative velocity interstitial velocity, $\mathbf{U}_g - \mathbf{U}_p$.

$$C_{Ds} = \left(0.63 + \frac{4.8}{\sqrt{\text{Re}_s}}\right)^2 \tag{17}$$

$$K = \frac{3\alpha_p(1 - \alpha_p)\rho_g}{4V_r^2 d_p}\left(0.63 + 4.8\sqrt{\left(\frac{V_r}{\text{Re}}\right)}\right)^2 |U_r| \tag{18}$$

The coefficients C_1 and C_2 in Eq. (16) are unique to a problem statement and depend on various parameters like Archimedes number, minimum fluidization velocity, and other physical properties of the individual phases. In our case, $C_1 = 0.88$ and $C_2 = 2.04$ which is calculated from previous equations. Existing Syamlal O'Brien drag correlation, Figure 2, was tuned with the new coefficients by creating a new drag model with the name *newSyamlalObrien,* Figure 3

```
// * * * * * * * * * * * * * * Member Functions  * * * * * * * * * * * * * * //

Foam::tmp<Foam::volScalarField> Foam::dragModels::SyamlalOBrien::CdRe() const
{
    volScalarField alpha2
    (
        max(scalar(1) - pair_.dispersed(), pair_.continuous().residualAlpha())
    );

    volScalarField A(pow(alpha2, 4.14));
    volScalarField B
    (
        neg(alpha2 - 0.85)*(0.8*pow(alpha2, 1.28))
      + pos0(alpha2 - 0.85)*(pow(alpha2, 2.65))
    );
```

Figure 2: Default code for Syamlal O'Brien in OpenFOAM

```
// * * * * * * * * * * * * * * Member Functions  * * * * * * * * * * * * * * //

Foam::tmp<Foam::volScalarField> Foam::dragModels::newSyamlalOBrien::CdRe() const
{
    volScalarField alpha2
    (
        max(scalar(1) - pair_.dispersed(), pair_.continuous().residualAlpha())
    );

    volScalarField A(pow(alpha2, 4.14));
    volScalarField B
    (
        neg(alpha2 - 0.85)*(0.88*pow(alpha2, 1.28))
      + pos0(alpha2 - 0.85)*(pow(alpha2, 2.04))
    );
```

Figure 3: Modified code of Syamlal O'Brien according to given parameters

3.2 Johnson & Jackson model

Unlike the fluid flow where a *noSlip* condition is applied to the walls, particles in a granular flow fluctuate between the two extremes of sticking to the wall and sliding on it. For the same reason, Johnson and Jackson developed boundary conditions [3] that relate the solid phase velocity with that of its granular temperature as shown in Eqs. (19) and (20).

$$\mu_s \frac{\partial u_s}{\partial x} = -\frac{\pi \phi_s \rho_s \alpha_s g_0 \sqrt{\theta_s}}{2\sqrt{3} \alpha_s^{max}} u_s \tag{19}$$

$$\kappa_s \frac{\partial \theta_s}{\partial x} = -\frac{\pi \phi_s u_s^2 \rho_s \alpha_s g_0 \sqrt{\theta_s}}{2\sqrt{3} \alpha_s^{max}} - \frac{\pi \sqrt{3} \rho_s \alpha_s g_0 (1 - e_W^2) \sqrt{\theta_s}}{4 \alpha_s^{max}} \theta_s \tag{20}$$

u_s and κ_s are viscosity and conductivity of solid phase, ϕ_s and e_W^1 are specularity coefficient and particle-wall coefficient of restitution. The granular temperature is made non-zero at t=0 in all the cells by defining a parameter called *referenceLevel* = 1e-4 in *Theta.particles* script file to avoid invalid mathematical operations. Table 2 contains the specularity coefficient and coefficient of restitution for particle – wall interactions considered in this case study.

Parameters	Value
Specularity coefficient (ϕ_s)	0.125 ($\mathbf{U}g = 2.19$) 0.05 ($\mathbf{U}g = 3.28$)
Particle – Wall restitution coefficient (e_W^1)	0.92

Table 2: KTGF Parameters

Effect of Specularity coefficient

Specularity coefficient (ϕ_s) is defined as the fraction of particle tangential momentum transferred to wall through collisions. It is an indicative of the wall roughness. This is affected by the superficial gas velocity and the particle size.

$$\phi_s = 1 \Rightarrow \text{Zero tangential velocity, maximum hindrance}$$
$$\phi_s = 0 \Rightarrow \text{Free slip along the wall, minimum hindrance}$$

In our problem, the specularity coefficient was considered as 0.05 for 3.28 m/s gas velocity [7] and 0.125 for 2.19 m/s gas velocity which yielded more accurate results.
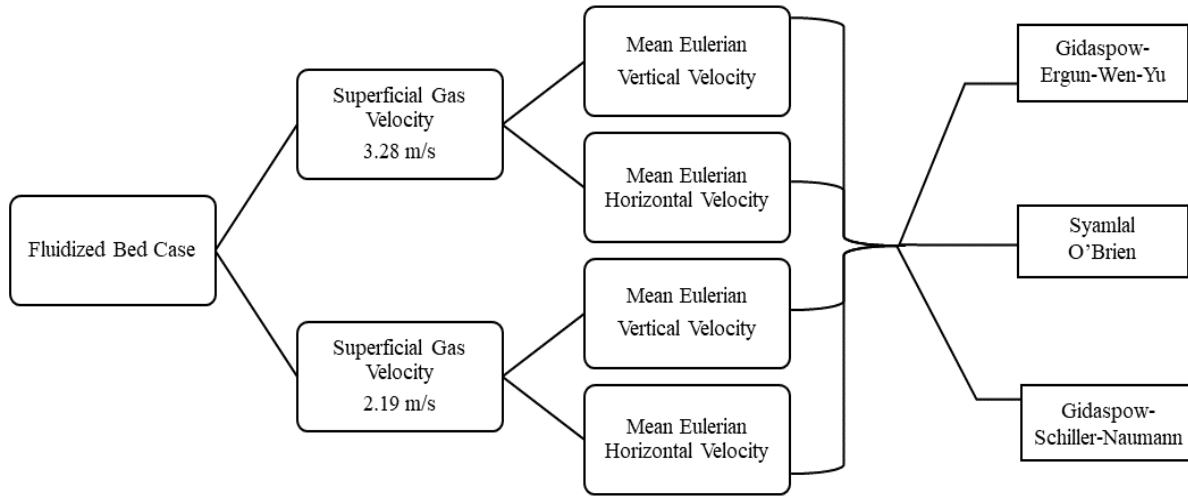
4. Simulation Procedure

Figure 4: Classification of the entire case study

The set of cases that are to be simulated in OpenFOAM for this study is shown in the form of a classification chart in Figure 4. The fluidized bed is a standard case study, readily existing in the tutorial directory of OpenFOAM under *twoPhaseEulerFoam* solver. Initially, the tutorial case file has to be copied into the run directory which is our working directory. The 0/constant/system folders containing various script files for defining the initial and boundary conditions, physical and phase properties, simulation control, and a few more are to be modified according to our requirements. Further, case files are accessed using the terminal to run the simulation using multiple commands.

After the simulation is complete, post-processing of the results is performed in ParaView, an open-source post-processing software. Particle velocity data at every timestamp is extracted by plotting the data over time for the required lateral location. The entire data obtained for all the cases are consolidated in one spreadsheet to plot the velocity distribution against lateral location for all three drag correlations. The results are compared with the experimental data generated by NETL [4] for validation and understanding the reliability of a drag correlation in modelling a dispersed multiphase simulation accurately.

4.1 Geometry and Mesh

The computational domain used to simulate the problem of the fluidized bed is shown in Figure 5. A 2D domain is chosen to make the multiphase simulation computationally less expensive. The dimensions of the domain are already marked in Figure 1. It is made sure that the edge dimensions of an element are larger than the diameter of the particle for the averaged Navier Stokes to be valid. *blockMesh* utility is used for geometry and hexahedral mesh generation.
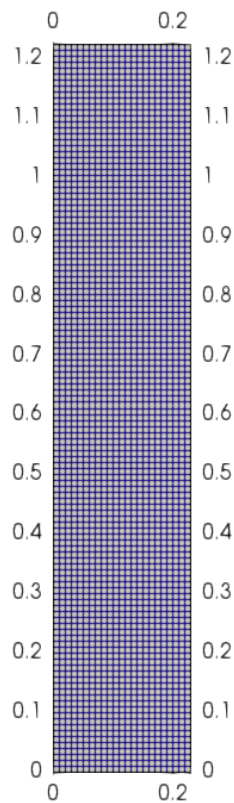
Direction	Number of divisions
X - axis	23
Y - axis	122
Z - axis	1

Table 3: Division of domain along the coordinate axis

Figure 5: 2D view of the computational domain

4.2 Initial and Boundary Conditions

The initial and boundary conditions of the field variables defined in Table 4-7 are of prime importance in defining how the flow develops inside the physical domain. The reason for defining *interstitialInletVelocity* condition over a *fixedValue* boundary condition for *U.air* is because of the transient nature of the simulation where the packing fraction of the phases keep changing with time. Similarly, *pressureInletOutletVelocity* is defined at the outlet for the flow to switch between *zeroGradient* and *fixedValue* conditions during the occurrence of a reverse flow.

Boundary	U.air (m/s)	U. particles (m/s)
Inlet	interstitialInletVelocity (0 2.19 0) & alpha.air	fixedValue (0 0 0)
Outlet	pressureInletOutletVelocity phi.air	fixedValue (0 0 0)
Walls	noSlip	JohnsonJacksonParticleSlip

Table 4: Velocity boundary conditions

Boundary	alpha	P_rgh	Theta
Inlet	zeroGradient	fixedFluxPressure	fixedValue
Outlet	zeroGradient	prghPressure p = 101325 Pa	zeroGradient
Walls	zeroGradient	fixedFluxPressure	JohnsonJacksonParticleTheta

Table 5: Miscellaneous boundary conditions

Boundary	T.air (m/s)	T. particles (m/s)
Inlet	zeroGradient	zeroGradient
Outlet	inletOutlet type	inletOutlet type
Walls	zeroGradient	zeroGradient

Table 7: Temperature boundary conditions

Boundary	k.air	epsilon.air	nut.air
Inlet	fixedValue	fixedValue	calculated
Outlet	inletOutlet	inletOutlet	calculated
Walls	kqRWallFunction	epsilonWallFunction	nutkWallFunction

Table 6: Turbulence boundary conditions

In a granular flow case, the particles neither stick to the wall nor slip freely on it. They oscillate between both these conditions and for the same reason, *JohnsonJacksonParticleSlip* condition is applied for the walls of both *U. particles* and *Theta.particles* field variables.

frontAndBackPlanes boundary is common for all field variables in the 0 folder. Since it is a 2D simulation problem, *empty* condition is defined for the boundary.

At t = 0, the column is filled with particles whose static bed height is 0.173m, as shown in Figure 1. Also, the initial packing fraction of the particles is 0.58 within the static bed and 0 in the remaining column volume. These non-uniform initial conditions are defined in the *setFields* utility of the *system* folder.

4.3 Solver

The *twoPhaseEulerFoam* is a Eulerian–Eulerian multiphase solver readily available in the open-source CFD toolbox, OpenFOAM. It is used for a system of 2 non-reacting compressible fluid phases, where one phase is always dispersed, making it a reliable solver for gas-solid fluidized systems and many other applications. It uses the Finite Volume Method (FVM) to solve cell-centred and phase-averaged governing equations. Each of the phases are treated as a continuum in this approach.

5. Results and Discussions

Post-processing of the results was carried out in ParaView and Excel. Particle velocity at different lateral locations was obtained by plotting the entire transient simulation over time for each lateral location to extract the velocity data at every time step for all 50 seconds. The extracted data was time-averaged in the time interval after a bubbling fluidization flow regime is established which is sustained till the end of the simulation. Figure 6 shows the contours for particle phase fraction at various time stamps for the Syamlal O'Brien drag correlation for the superficial gas velocity of 2.19 m/s.
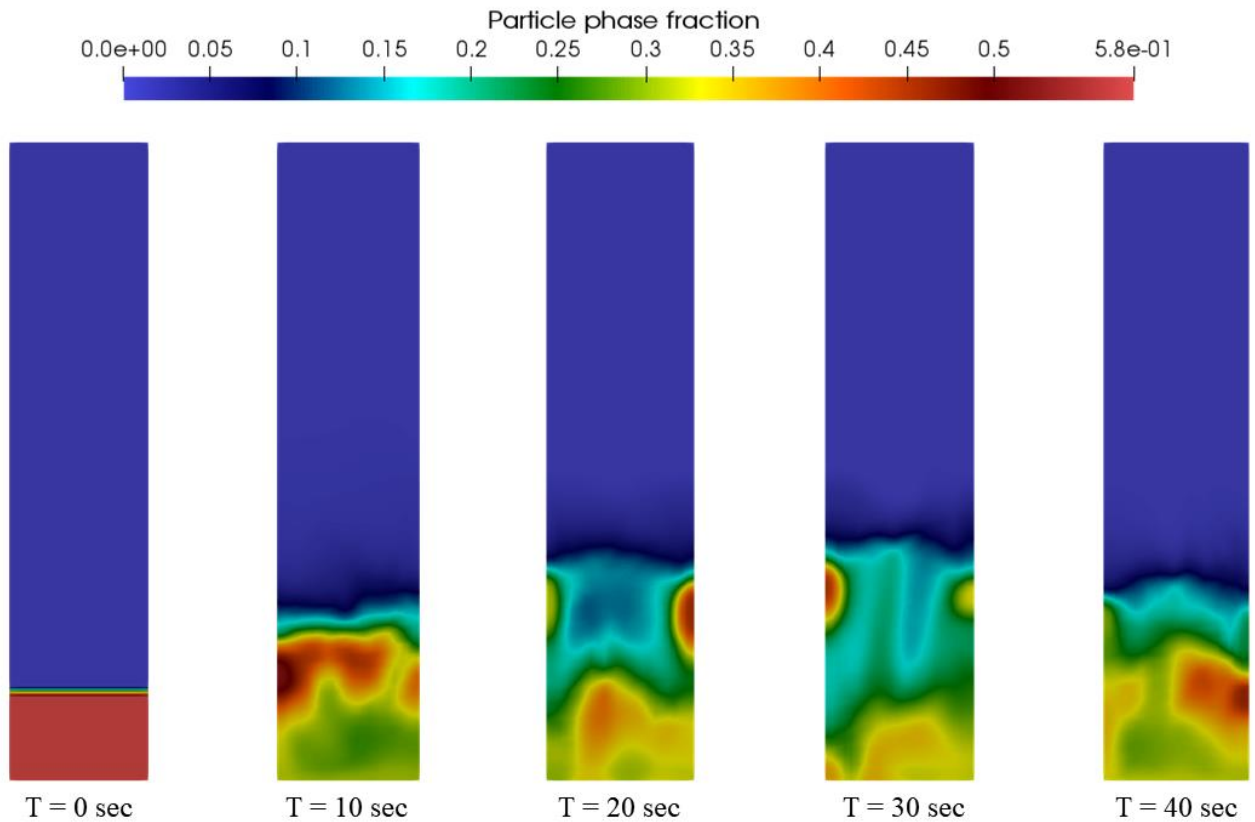

Figure 6: Contours of particle phase fraction (α_p) at five different timestamps

5.1 Result 1: Mean Eulerian Vertical Velocity Distribution (for Ug= 2.19 m/s)
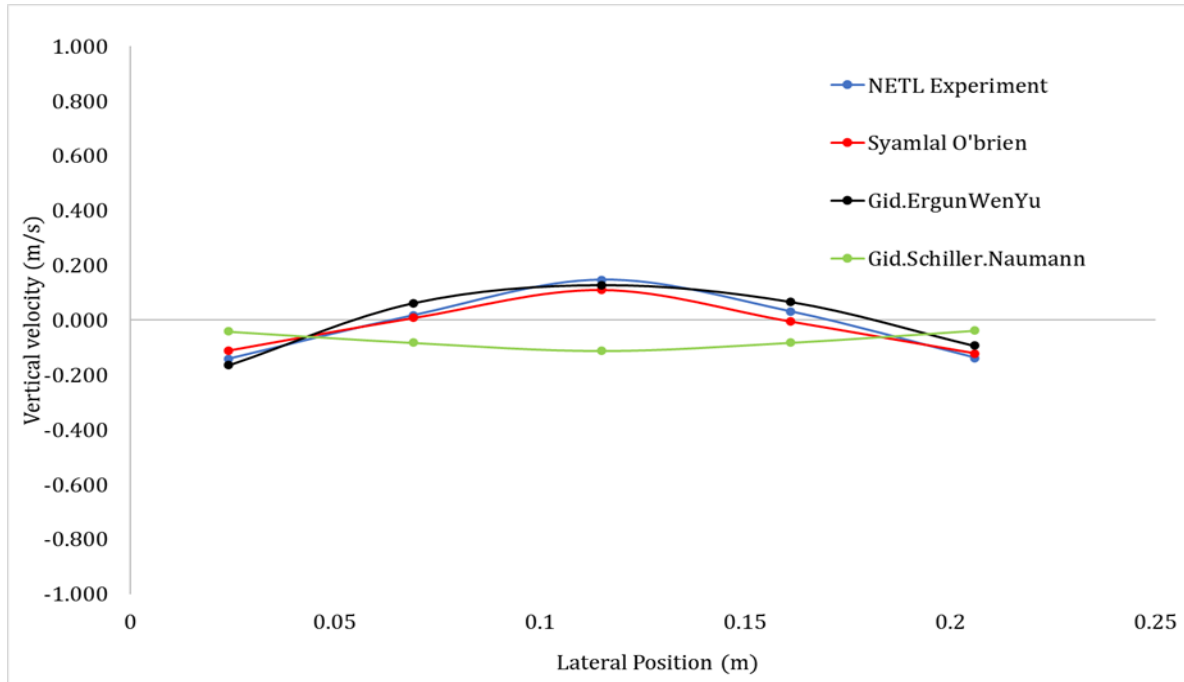

Figure 7: Vertical velocity vs Lateral position plot for various drag correlations (U_g= 2.19 m/s)

X	NETL Experiment	Syamlal O'Brien	Rel. Error wrt Expt	GEW	Rel. Error wrt Expt	GSN	Rel. Error wrt Expt
0.024	-0.142	-0.111	0.216	-0.164	0.746	-0.042	0.707
0.069	0.017	0.008	0.531	0.062	1.990	-0.083	5.855
0.115	0.147	0.111	0.599	0.128	0.469	-0.112	1.762
0.161	0.031	-0.005	1.156	0.066	0.075	-0.082	3.646
0.206	-0.138	-0.122	0.118	-0.094	0.280	-0.038	0.724

Table 10: Relative error in velocity measurements of drag models wrt. experimental results

The time-averaged vertical velocity data of the particles at five different lateral locations of the fluidized bed is plotted in Figure 7 for different drag correlations. Experimental data generated by NETL for the same is included for comparison with the CFD results. The velocity distribution obtained for Syamlal O'Brien drag correlation is almost overlapping with that of the experimental data followed by Gidaspow-Ergun-Wen-Yu (GEW). The trend of experimental results is followed by both Syamlal O'Brien and GEW but not by Gidaspow-Schiller Naumann (GSN). The time-averaged vertical velocity is the highest at the central location for all correlations except GSN. Therefore, we can comfortably infer that the Syamlal O'Brien correlation is most accurate in emulating the results obtained experimentally over other correlations for a superficial gas velocity of 2.19 m/s.

5.2   Result 2: Mean Eulerian Horizontal Velocity Distribution (for U_g= 2.19
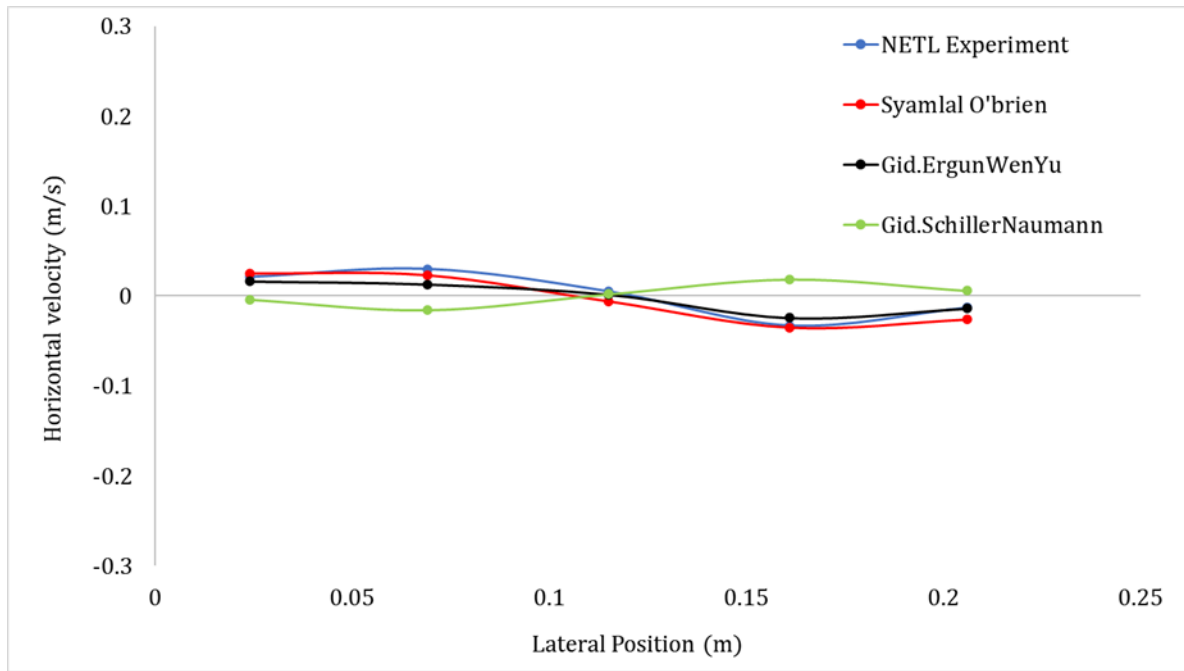

Figure 8: Horizontal velocity vs Lateral position plot for various drag correlations ($\mathbf{U}_g$= 2.19 m/s)

m/s)

X	NETL Experiment	Syamlal O'Brien	Rel. Error wrt Expt	GEW	Rel. Error wrt Expt	GSN	Rel. Error wrt Expt
0.024	0.021	0.025	0.179	0.016	0.543	-0.004	1.188
0.069	0.03	0.023	0.241	0.013	0.872	-0.016	1.530
0.115	0.005	-0.006	2.214	0.002	2.893	0.002	0.618
0.161	-0.033	-0.035	0.065	-0.024	0.001	0.019	1.562
0.206	-0.013	-0.026	1.016	-0.014	1.124	0.006	1.446

Table 9: Relative error in velocity measurements of drag models wrt. experimental results

The results obtained for horizontal velocity distribution, Figure 8, further strengthen our inference made from the vertical velocity results about the accuracy of the Syamlal O'Brien correlation because of its overlapping with the experimental results. However, GEW has performed almost as good as Syamlal correlation for the 2.19 m/s superficial gas velocity. Similar to the vertical velocity distribution, the GSN correlation fails to follow the trend of other plots despite the low relative error as shown in Table 9.

5.3   Result 3: Mean Eulerian Vertical Velocity Distribution (for $\mathbf{U}_g$= 3.28 m/s)
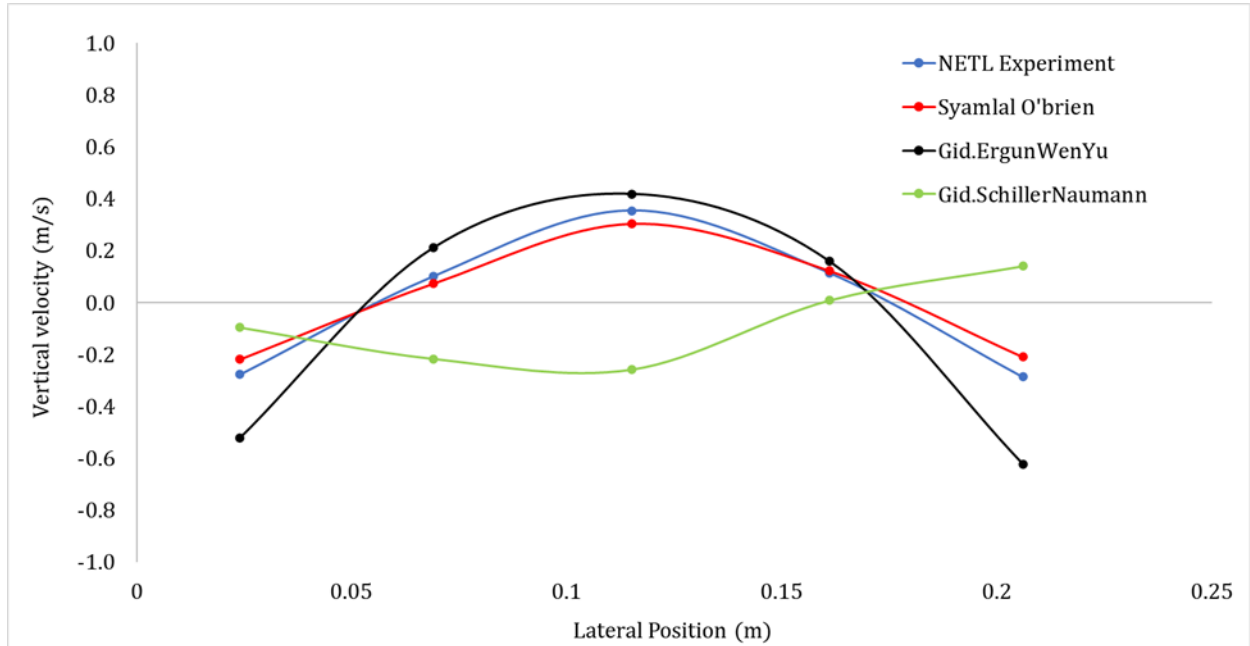

Figure 9: Vertical velocity vs Lateral position plot for various drag correlations ($\mathbf{U}_g$= 3.28 m/s)

X	NETL Experiment	Syamlal O'Brien	Rel. Error wrt Expt	GEW	Rel. Error wrt Expt	GSN	Rel. Error wrt Expt
0.024	-0.277	-0.220	0.672	-0.522	0.119	-0.096	0.652
0.069	0.101	0.073	0.684	0.212	2.519	-0.217	3.150
0.115	0.354	0.304	0.817	0.419	0.869	-0.259	1.731
0.161	0.114	0.122	0.714	0.159	0.641	0.008	0.929
0.206	-0.287	-0.210	0.441	-0.623	0.874	0.140	1.490

Table 10: Relative error in velocity measurements of drag models wrt. experimental results

Interesting behaviour was observed in the time-averaged vertical velocity distribution when the superficial gas velocity was increased from 2.19 m/s to 3.28 m/s as shown in Figure 9. Syamlal correlation again proved to be the accurate among others, though the relative error has slightly increased when compared to the 2.19 m/s vertical velocity distribution. The direction of velocity at the five lateral locations for both GEW and Syamlal correlation happens to be same as that of experimental observations which is not the case with GSN. Though GEW correlation has managed to successfully follow the trend of experimental results, the first and last lateral location values are highly deviating for GEW relative to Syamlal. Except for the first lateral location, the velocity direction was completely opposite to that of the experiment for GSN correlation.

5.4   Result 4: Mean Eulerian Horizontal Velocity Distribution (for U_g= 3.28 m/s)
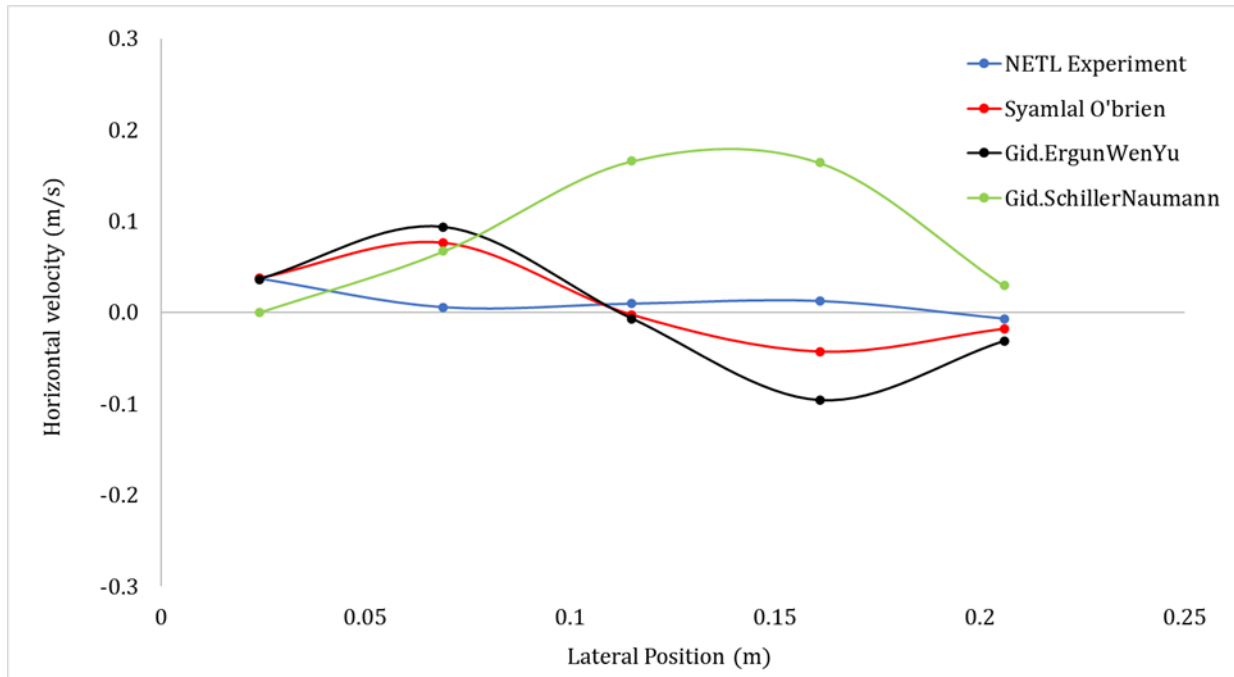

Figure 10: Horizontal velocity vs Lateral position plot for various drag correlations (U_g= 3.28

X	NETL Experiment	Syamlal O'Brien	Rel. Error wrt Expt	GEW	Rel. Error wrt Expt	GSN	Rel. Error wrt Expt
0.024	0.037	0.038	0.526	0.036	0.956	0.000	1.006
0.069	0.005	0.076	5.779	0.093	27.558	0.067	11.423
0.115	0.009	-0.003	1.273	-0.007	8.656	0.166	16.893
0.161	0.012	-0.043	4.526	-0.096	3.264	0.164	12.421
0.206	-0.007	-0.018	1.511	-0.032	2.482	0.029	5.056

Table 11: Relative error in velocity measurements of drag models wrt. experimental results

At a particular lateral location, the CFD results obtained for the horizontal velocity, deviated more from the corresponding experimental values as depicted in Figure 10 when compared to the results that were obtained for the 2.19 m/s gas velocity. Surprisingly, the trend observed in experimental results was not followed by the drag correlations but, a similar trend was observed in the work of [5] for same values of gas velocity and similar drag correlations. Thus, the trend followed by Syamlal and GEW is what is expected out of a CFD simulation. However, GSN totally overpredicts the velocity at all lateral locations like it has performed for other cases as well.

The first major inference that can be drawn from the results is that, out of the three drag correlations, the Gidaspow-Schiller-Naumann correlation predicted the particle velocity distributions poorly for both the cases of gas velocity. Despite being developed to account for the particle-particle interactions by including the voidage function, it was least accurate for both the velocity cases. This can be attributed to the fact that it was primarily developed for packed bed applications where the gas velocity is relatively low, restricting the flow regime to a fixed bed. The drastic increase in relative error as the gas velocity is raised from 2.19 m/s to 3.28 m/s for the GSN correlation reinforces our inference about the better performance of the GSN correlation at low fluid velocities and dilute particle concentrations.

Initially, vertical velocity profiles deviated the maximum from the experimental counterparts at the central location for all the drag models. After changing the specularity coefficient from 0.5 to 0.125 for 2.19 m/s case and 0.5 to 0.05 for 3.28 m/s case, the required bump in the vertical velocity at central location was observed for both GEW and Syamlal drag correlations. Low values of specularity coefficient produce high particle velocities in the bed as there is less loss of tangential momentum to the walls [7].

Finally, Syamlal O'Brien's drag correlation performed exceptionally well in replicating the experimental results for both the gas velocities. The reason for this realistic behaviour could be because of the consideration of the clustering effect [6] of particles in the model, unlike other correlations. Gidaspow-Ergun-Wen-Yu drag correlation performed on par with the Syamlal model at lower gas velocity. As the gas velocity was increased to 3.28 m/s, though the trend in both horizontal and vertical velocities was replicated exactly, a higher relative error than that of the Syamlal model makes it unsuitable at higher velocities.

Conclusion

This study was performed to identify the most reliable drag correlation for computational modelling of dispersed Multiphase flows in a fluidized bed. The CFD results of particle velocity profiles obtained for different drag correlations were compared with the experimental data. Syamlal O'Brien drag correlation outperformed others for both the cases of superficial gas velocity, 2.19 m/s and 3.28 m/s, by accurately predicting the Mean Eulerian particle velocity distributions at various lateral locations of the fluidized bed. The Gidaspow-Ergun-Wen-Yu correlation's predictions were on par with the former for lower gas velocity of 2.19 m/s but are only satisfactory for the 3.28 m/s gas velocity case. The Gidaspow-Schiller-Naumann correlation was least accurate among the three in predicting the velocity profile but has given useful insights about the model and its operating range.

Analysing the effect of fluid phase turbulence models on the flow structure can further aid this study in choosing the right combination of drag and turbulence correlations for accurate modelling of dispersed multiphase flows.

References

[1] H, Enwald, E. Peirano, A-E Almstedt 'Eulerian Two-Phase Flow Theory Applied to Fluidization' Int. J. Multiphase Flow, Vol. 22, Suppl, pp. 21-66, 1996

[2] Ding, J. and Gidaspow, D. A bubbling fluidization model using kinetic theory of granular flow. AIChE Journal 36, 523-538, 1990

[3] Johnson, P. C., & Jackson, R. Frictional–collisional constitutive relations for granular materials, with application to plane shearing. Journal of Fluid Mechanics, 176(-1), 67, 1987

[4] National Energy Technology Laboratory (NETL). (2013, May 30). Small Scale Challenge Problem I (2013). https://mfix.netl.doe.gov/experimentation/challenge-problems/small-scale-challenge-problem-i-2013/

[5] Sobieski, W.: Drag Coefficient in Solid-Fluid System Modelling with the Eulerian Multiphase Model. Drying Technol., 2011. Vol. 29, pp. 111-125.

[6] O'Brien, T. J. and Syamlal, M. Particle cluster effects in the numerical simulation of a circulating fluidized bed. 4th Int. Conf. on CFB, Somerset, USA, Preprint Volume, pp. 430—435, 1993

[7] Lungu, M., Wang, H., Wang, J., Yang, Y., & Chen, F. Two-Fluid Model Simulations of the National Energy Technology Laboratory Bubbling Fluidized Bed Challenge Problem. Industrial & Engineering Chemistry Research, 55(17), 5063–5077, 2016